Inverse scattering with diffusing waves

John C. Schotland and Vadim A. Markel

Department of Electrical Engineering, Washington University, St. Louis, Missouri 63130

Received June 22, 2000; revised manuscript received April 13, 2001; accepted April 26, 2001

We consider the problem of imaging the optical properties of a highly scattering medium probed by diffuse light. An analytic solution to this problem is derived from the singular value decomposition of the forward-scattering operator, which leads to explicit inversion formulas for the inverse scattering problem with diffusing waves. Computer simulations are used to illustrate these results in model systems. © 2001 Optical Society of America

OCIS code: 290.0290.

1. INTRODUCTION

There has been considerable recent interest in the problem of developing tomographic methods for imaging in highly scattering systems.[1–7] In such systems multiple scattering of light leads to the breakdown of geometrical optics and presents a fundamental physical obstruction to optical imaging. Two conceptually different approaches to this problem are currently under investigation. In the first approach, referred to as ballistic imaging, unscattered photons are selected by an optical gate and are then used for image formation.[1–6] The intensity of such unscattered radiation is highly attenuated, and thus this approach is subject to practical limitations beyond which there is no way to improve its performance. The second, more powerful approach is to directly use the scattered radiation for image reconstruction.[7–21] Here, in the usual formulation of the image reconstruction problem, the diffusive nature of multiply scattered light is exploited to effect an approximate inversion of the forward-scattering problem by a numerical method. This approach, however, is severely limited by the computational complexity of the inversion procedure.

In this paper we describe an analytic inverse scattering method that may be used to reconstruct the optical absorption and diffusion coefficients of a highly scattering system probed by diffusive light. The physical situation that we consider is illustrated in Fig. 1, where a diffusing wave is incident upon a highly scattering object. The intensity of the scattered wave is measured on a surface adjacent to the object and is used as the data in the inverse scattering procedure. The solution to the inverse problem is then obtained in the form of explicit inversion formulas. The starting point for this development is the analytic construction of the singular value decomposition (SVD) of the linearized forward-scattering operator. The SVD provides a precise characterization of the inverse problem and leads to an image reconstruction algorithm with distinct computational advantages. In particular, the computational complexity scales as $O(N \log N)$, where N is the number of measurements (source–detector pairs).

The inversion procedure that is described in this paper is applicable to imaging in many highly scattering systems in which the transport of light may be regarded as diffusive. Such systems are ubiquitous in nature and include biological tissue, the ocean, the atmosphere, and interstellar media. Diffusion tomography refers to a form of biomedical imaging that utilizes near-infrared diffuse light to image tissue structure while simultaneously obtaining physiologically and functionally important spectroscopic information. A clinical application of current interest is the imaging of tissue oxygenation in tumors.

It is important to note that although the main focus of this work is the inverse scattering problem for diffuse light, the results presented are, in fact, very general. Similar equations describe the propagation of heat in a body with fluctuating thermal conductivity or the flow of steady current in a medium with fluctuating electrical conductivity. In both situations the proposed solution to the inverse problem can be used to reconstruct the distribution of these conductivities from an appropriate set of measurements.

This paper is organized as follows. In Section 2 we derive the integral equations that describe the forward-scattering problem within the diffusion approximation. In Section 3 we consider the image reconstruction problem in the backscattering geometry as a means of introducing the methods that are further developed in Section 4 to treat the general inverse problem. Computer simulations illustrating the image reconstruction algorithm are presented in Section 5.

2. INTEGRAL EQUATIONS

Consider an experiment in which light propagates in a highly scattering medium characterized by an optical absorption coefficient $\alpha(r)$ and a photon diffusion coefficient $D(r)$. In this situation the transport of light can be regarded as occurring by means of a diffusing wave whose energy density $u(r, t)$ satisfies the equation

$$\partial_t u(r, t) = \nabla \cdot [D(r)\nabla u(r, t)] - \alpha(r)u(r, t) + S(r, t), \tag{1}$$

where $S(r, t)$ is the power density of the source. If the source is amplitude modulated at frequency ω, then

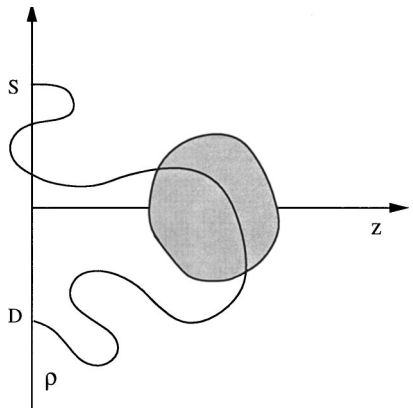

Fig. 1. Experimental geometry. The sample occupies the half-space $z > 0$ of an infinite medium with sources and detectors located on the plane $z = 0$ with transverse coordinate ρ. A typical photon path is also shown.

$$S(r,t) = [1 + A\exp(-i\omega t)]S(r), \tag{2}$$

where $S(r)$ is the unmodulated source power density and $A \leqslant 1$. If $u(r,t)$ is decomposed into a zero-frequency component $u_0(r)$ and a frequency-dependent component $u(r)$ by

$$u(r,t) = u_0(r) + A\exp(-i\omega t)u(r), \tag{3}$$

then $u(r)$ obeys the equation

$$-\nabla \cdot [D(r)\nabla u(r)] + [\alpha(r) - i\omega]u(r) = S(r). \tag{4}$$

It is important to note that the case of pulsed sources with $S(r,t) = S(r)\delta(t)$ is also readily treated. In this case the Fourier transform of $u(r,t)$ with respect to t leads directly to $u(r)$.

The solution to Eq. (4) may be expressed in terms of the diffusion Green's function $G(r,r')$ and is given by

$$u(r) = \int \mathrm{d}^3r'\, G(r,r')S(r'), \tag{5}$$

where $G(r,r')$ satisfies the equation

$$[-\nabla_r \cdot D(r)\nabla_r + \alpha(r) - i\omega]G(r,r') = \delta(r - r'). \tag{6}$$

In an infinite homogeneous medium with absorption α_0 and diffusion constant D_0, the Green's function $G_0(r,r')$ is given by

$$G_0(r_1,r_2) = \frac{\exp(-k_0|r_1 - r_2|)}{4\pi D_0|r_1 - r_2|}, \tag{7}$$

where the wave number

$$k_0^2 = \frac{\alpha_0 - i\omega}{D_0}. \tag{8}$$

For later reference we provide the plane-wave decomposition of $G_0(r_1,r_2)$, which is of the form

$$G_0(r,r') = \frac{1}{2D_0}\int \frac{\mathrm{d}^2q}{(2\pi)^2}Q(q)^{-1} \times \exp[iq \cdot (\rho - \rho') - Q(q)|z - z'|], \tag{9}$$

where $r = (\rho, z)$ and $r' = (\rho', z')$. This result follows from the Fourier integral representation of $G_0(r_1,r_2)$,

$$G_0(r,r') = \frac{1}{D_0}\int \frac{\mathrm{d}^3k}{(2\pi)^3}\frac{\exp[ik \cdot (r - r')]}{k^2 + k_0^2}, \tag{10}$$

and the identity

$$\int_{-\infty}^{\infty}\frac{\exp(ik_zz)}{k_z^2 + q^2 + k_0^2}\mathrm{d}k_z = \frac{\pi}{Q(q)}\exp[-Q(q)|z|], \tag{11}$$

where

$$Q(q) \equiv (q^2 + k_0^2)^{1/2}. \tag{12}$$

With the use of standard perturbative methods, the Green's function may be obtained from the Dyson equation

$$G(r_1,r_2) = G_0(r_1,r_2) - \int \mathrm{d}^3r[G_0(r_1,r)G(r,r_2)\delta\alpha(r) + \nabla_rG_0(r_1,r) \cdot \nabla_rG(r,r_2)\delta D(r)], \tag{13}$$

where $G_0(r_1,r_2)$ is the unperturbed Green's function for a homogeneous reference medium with absorption α_0 and diffusion coefficient D_0. Here $\delta\alpha(r) = \alpha(r) - \alpha_0$ and $\delta D(r) = D(r) - D_0$ denote the spatial fluctuations in the absorption and diffusion coefficients away from their values in the reference medium.

The transmission $T(r_1,r_2)$ of a diffusing wave that is generated by a point source at r_1 and is detected at r_2 is defined as the transmitted intensity of the frequency-dependent component of the wave normalized by the intensity that would be measured in the reference medium. Equation (13) may be used to obtain an integral equation for the transmission of the form

$$T(r_1,r_2) = 1 - \frac{1}{G_0(r_1,r_2)} \times \int \mathrm{d}^3r[G_0(r_1,r)G(r,r_2)\delta\alpha(r) + \nabla_rG_0(r_1,r) \cdot \nabla_rG(r,r_2)\delta D(r)]. \tag{14}$$

Equation (14) is an exact expression for the transmission that may be used to generate a perturbation expansion in $\delta\alpha(r)$ and $\delta D(r)$. This expansion is analogous to the Born series and, to lowest order in $\delta\alpha(r)$ and $\delta D(r)$, leads to the Born approximation.[18] Standard diagrammatic techniques (as shown in Fig. 2) may be used to resum this expansion, with the result that, to first order in $\delta\alpha$ and δD,

$$-\ln T(r_1,r_2) = \int \mathrm{d}^3r[\Gamma_A(r;r_1,r_2)\delta\alpha(r) + \Gamma_D(r;r_1,r_2)\delta D(r)], \tag{15}$$

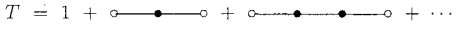

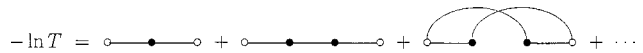

Fig. 2. Diagrammatic expansions of T and $\ln T$. The solid lines indicate a factor of G_0, the black circles represent a factor of $\delta\alpha$ weighted by the appropriate combinatorial factors, with the internal coordinates integrated, and the white circles indicate an unintegrated coordinate.

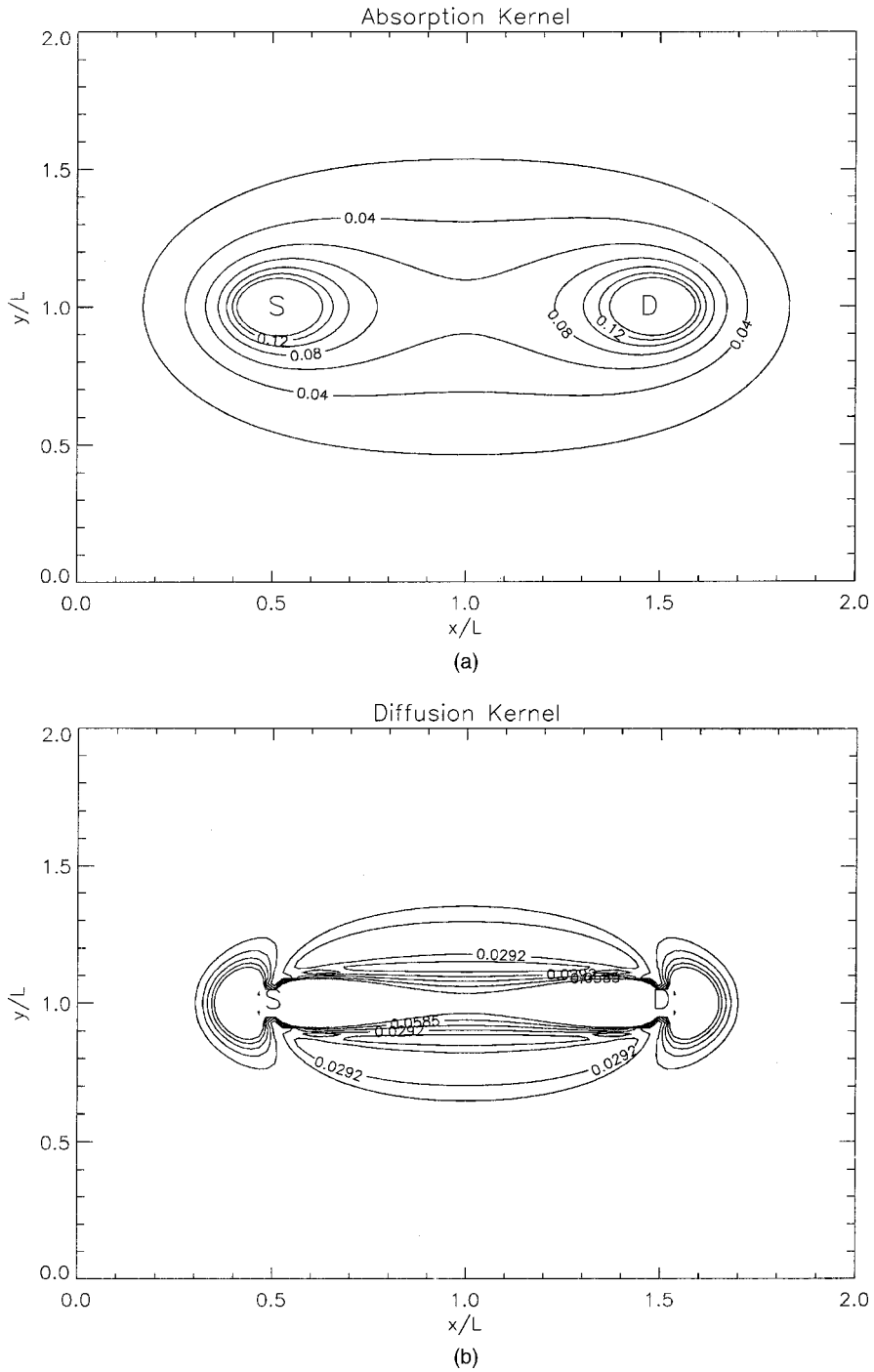

Fig. 3. Contour plots of (a) Γ_A and (b) Γ_D in an infinite nonabsorbing medium for $k_0L = 1$, where L denotes the source–detector pair separation.

where the absorption kernel

$$\Gamma_A(r;r_1,r_2) = -\frac{\delta \ln T(r_1,r_2)}{\delta \alpha(r)}\bigg|_{\delta\alpha(r)=0,\delta D(r)=0}$$

$$= \frac{1}{G_0(r_1,r_2)} G_0(r_1,r) G_0(r,r_2) \qquad (16)$$

and the diffusion kernel

$$\Gamma_D(r;r_1,r_2) = -\frac{\delta \ln T(r_1,r_2)}{\delta D(r)}\bigg|_{\delta\alpha(r)=0,\delta D(r)=0}$$

$$= \frac{1}{G_0(r_1,r_2)} \nabla_r G_0(r_1,r) \cdot \nabla_r G_0(r,r_2). \qquad (17)$$

Contour plots of $\Gamma_A(r;r_1,r_2)$ and $\Gamma_D(r;r_1,r_2)$ in an infinite medium are shown in Fig. 3. Equation (15) provides an explicit solution to the forward problem in diffusion to-

mography in the form of an integral equation that relates $T(r_1, r_2)$ to $\delta\alpha(r)$ and $\delta D(r)$.

3. INVERSE PROBLEM

In the diffusive inverse scattering problem, we wish to reconstruct the absorption and diffusion coefficients from the intensity of the diffusing wave measured on a surface adjacent to the sample. The approach to this problem described here leads to the construction of explicit inversion formulas for the integral equation (15) by constructing the SVD of the forward-scattering operator. For simplicity we consider an infinite medium in which the sources and detectors are located on the plane $z = 0$. Other geometries are also readily treated. To this end we denote by ρ_1 and ρ_2 the transverse coordinates of the source and detector, and we put $\phi(\rho_1, \rho_2) = -(G_0(\rho_1, 0;\rho_2, 0)\ln T(\rho_1, 0;\rho_2, 0)$. In this notation Eq. (15) may be rewritten as an integral equation for the scattering data $\phi(\rho_1, \rho_2)$, which is given by

$$\phi(\rho_1, \rho_2) = \int d^3r[G_0(\rho_1, 0;r)G_0(\rho_2, 0;r)\delta\alpha(r) + \nabla_r G_0(\rho_1, 0;r) \cdot \nabla_r G_0(\rho_2, 0;r)\delta D(r)]. \tag{18}$$

The image reconstruction problem now consists of solving the integral equation (18) for $\delta\alpha(r)$ and $\delta D(r)$ when $\phi(\rho_1, \rho_2)$ is specified.

We introduce the Fourier transform with respect to ρ_2 of the scattering data, which is defined by

$$\phi_q(\rho_1) = \int d^2\rho_2 \exp(iq \cdot \rho_2)\phi(\rho_1, \rho_2). \tag{19}$$

Thus Eq. (18) becomes

$$\phi_q(\rho_1) = \int d^3r[K_q^A(\rho_1, r)\delta\alpha(r) + K_q^D(\rho_1, r)\delta D(r)], \tag{20}$$

where

$$K_q^A(\rho_1, r) = \frac{1}{2D_0Q(q)}\exp[iq \cdot \rho - Q(q)|z|] \times G_0(\rho_1, 0;r), \tag{21}$$

$$K_q^D(\rho_1, r) = \frac{1}{2D_0Q(q)}\exp[iq \cdot \rho - Q(q)|z|] \times [i\mathbf{q} - Q(q)\hat{z}] \cdot \nabla_r G_0(\rho_1, 0;r) \tag{22}$$

with $\mathbf{q} = (q, 0)$. It is important to observe that the descriptions of the scattering experiment in terms of $\phi_q(\rho_1)$ or $\phi(\rho_1, \rho_2)$ are equivalent. Thus $\delta\alpha(r)$ and $\delta D(r)$ can be reconstructed from either of the integral equations (18) or (20). Starting from the latter integral equation, we describe two approaches to this problem. In the first approach, for a single fixed value of the wave vector q, we construct the SVD of the operators $K_q^{A,D}(\rho_1, r)$ and use this result to solve the integral equation (20). In this situation, however, a difficulty arises; namely, $\delta\alpha(r)$ and $\delta D(r)$, which are functions of three variables, are to be reconstructed from $\phi_q(\rho_1)$, a function of two variables. As a consequence, the single-wave-vector form of the inverse problem is severely ill-posed and leads to reconstructions with poor depth-dependent resolution. Note that in the special case in which the medium is separable, a single wave vector suffices, consistent with the results of others.[22,23] In the second approach, we systematically improve upon the first by making use of the scattering data for a finite number of wave vectors. This overcomes the problem of recovering three-dimensional information from two-dimensional data.

A. Single-Wave-Vector Solutions

In this subsection we consider the reconstruction of the absorption and diffusion coefficients from the scattering data $\phi_q(\rho_1)$ for a fixed value of the wave vector q. We first discuss the problem of reconstructing the absorption in a medium with a spatially uniform diffusion coefficient. In this situation $\phi_q(\rho_1)$ satisfies the integral equation

$$\phi_q(\rho_1) = \int d^3r\, K_q^A(\rho_1, r)\delta\alpha(r). \tag{23}$$

To proceed, we require the SVD of the operator $K_q^A(\rho_1, r)$. To this end the identity (9) may be used to express $K_q^A(\rho_1, r)$ as

$$K_q^A(\rho_1, r) = \int d^2q'\, \sigma_{q'q}^A g_{q'q}(\rho_1) f_{q'q}^{A*}(r), \tag{24}$$

where the singular functions are given by

$$g_{q'q}(\rho) = \frac{1}{2\pi}\exp[i(q + q') \cdot \rho], \tag{25}$$

$$f_{q'q}^A(r) = \frac{N_{q'q}}{2\pi}\exp(i(q' \cdot \rho + \theta_{q'q}^A) - \{[Q(q)]^* + [Q(q + q')]^*\}|z|), \tag{26}$$

with the corresponding singular values

$$\sigma_{q'q}^A = \frac{1}{4D_0^2 N_{q'q}|Q(q)Q(q + q')|}. \tag{27}$$

Here $N_{q'q}$ is an appropriate normalization factor (whose explicit form we will not require), chosen so that $\langle f_{q'q}^A, f_{q''q}^A\rangle = \delta(q' - q'')$, and the phase factor is given by

$$\exp(i\theta_{q'q}^A) = \frac{Q(q)Q(q + q')}{|Q(q)Q(q + q')|}. \tag{28}$$

It is readily verified that Eq. (24) defines the SVD of $K_q^A(\rho_1, r)$, since

$$K_q^{A*}K_q^A f_{q'q}^A = (\sigma_{q'q}^A)^2 f_{q'q}^A, \tag{29}$$

$$K_q^A f_{q'q}^A = \sigma_{q'q}^A g_{q'q}. \tag{30}$$

The SVD (24) may now be used to obtain the solution to the integral equation (23). Since $\delta\alpha$ and ϕ_q belong to different Hilbert spaces, a solution to the equation $K_q^A\delta\alpha = \phi_q$ is defined to be a minimizer of $\|K_q^A\delta\alpha - \phi_q\|$. Among all such solutions, it is conventional to choose the one with minimum L^2 norm.[24] This so-called generalized solution is unique and is given by

$$\delta\alpha(r) = \int \mathrm{d}^2\rho_1 K_q^{A+}(r, \rho_1)\phi_q(\rho_1), \tag{31}$$

where the generalized inverse of K_q^A is given by

$$K_q^{A+}(r, \rho_1) = \int \mathrm{d}^2q' \frac{1}{\sigma_{q'q}^A} g_{q'q}^*(\rho_1) f_{q'q}^A(r). \tag{32}$$

We now turn to the problem of reconstructing the diffusion coefficient of a medium with a spatially uniform absorption coefficient. Equation (20) thus becomes

$$\phi_q(\rho_1) = \int \mathrm{d}^3r\, K_q^D(\rho_1, r)\delta D(r). \tag{33}$$

As above, it follows that $K_q^D(\rho_1, r)$ is given by the SVD

$$K_q^D(\rho_1, r) = \int \mathrm{d}^2q'\, \sigma_{q'q}^D g_{q'q}(\rho_1) f_{q'q}^{D*}(r) \tag{34}$$

with the singular values

$$\sigma_{q'q}^D = \sigma_{q'q}^A |q \cdot (q + q') + Q(q)Q(q + q')| \tag{35}$$

and $f_q^D(r) = \exp(i\theta_{q'q}^D) f_q^A(r)$. Here the phase $\theta_{q'q}^D$ is defined by

$$\exp(i\theta_{q'q}^D) = \frac{q \cdot (q + q') + Q(q)Q(q + q')}{|q \cdot (q + q') + Q(q)Q(q + q')|} \times \exp(i\theta_{q'q}^A). \tag{36}$$

Thus the solution to the integral equation (33) is given by

$$\delta D(r) = \int \mathrm{d}^2\rho_1 K_q^{D+}(r, \rho_1)\phi_q(\rho_1), \tag{37}$$

where

$$K_q^{D+}(r, \rho_1) = \int \mathrm{d}^2q' \frac{1}{\sigma_{q'q}^D} g_{q'q}^*(\rho_1) f_{q'q}^D(r). \tag{38}$$

Finally, we consider the general case of reconstructing both the absorption and diffusion coefficients. We require the solution to the integral equation (20), which is given by

$$\delta\alpha = K_q^{A*}(K_q^A K_q^{A*} + K_q^D K_q^{D*})^{-1}\phi_q, \tag{39}$$

$$\delta D = K_q^{D*}(K_q^A K_q^{A*} + K_q^D K_q^{D*})^{-1}\phi_q. \tag{40}$$

Since $K_q^A K_q^{A*}$ and $K_q^D K_q^{D*}$ commute, we may now use the SVDs of K_q^A and K_q^D to rewrite Eqs. (39) and (40) as

$$\delta\alpha(r) = \int \mathrm{d}^2\rho_1 \int \mathrm{d}^2q'\, \sigma_{q'q}^A [(\sigma_{q'q}^A)^2 + (\sigma_{q'q}^D)^2]^{-1} \times g_{q'q}^*(\rho_1) f_{q'q}^A(r)\phi_q(\rho_1), \tag{41}$$

$$\delta D(r) = \int \mathrm{d}^2\rho_1 \int \mathrm{d}^2q'\, \sigma_{q'q}^D [(\sigma_{q'q}^A)^2 + (\sigma_{q'q}^D)^2]^{-1} \times g_{q'q}^*(\rho_1) f_{q'q}^D(r)\phi_q(\rho_1), \tag{42}$$

which is the inversion formula for the inverse problem with scattering data determined by a single wave vector.

B. Multiple-Wave-Vector Solutions by Singular Value Decomposition

In this subsection we consider the reconstruction of $\delta\alpha$ and δD from p measurements of $\phi_q(\rho_1)$ corresponding to the wavevectors $q = q_1, \ldots, q_p$. The image reconstruction problem thus consists of solving the system of integral equations

$$K_{q_i}^A \delta\alpha + K_{q_i}^D \delta D = \phi_{q_i} \tag{43}$$

with $i = 1, \ldots, p$. Equation (43) can be rewritten in the form

$$Kf = \phi, \tag{44}$$

where

$$K = \begin{bmatrix} K_{q_1}^A & K_{q_i}^D \\ \vdots & \vdots \\ K_{q_p}^A & K_{q_p}^D \end{bmatrix}, \tag{45}$$

$f = (\delta\alpha, \delta D)^{\mathrm{T}}$, and $\phi = (\phi_{q_1}, \ldots, \phi_{q_p})^{\mathrm{T}}$. The solution to Eq. (44) follows from the SVD of the operator $K(\rho_1, r)$, which is given by

$$K(\rho_1, r) = \int \mathrm{d}^2q \sum_{l=1}^{p} \sigma_{ql}\phi_{ql}(\rho_1)\psi_{ql}^*(r). \tag{46}$$

Here the singular functions $\phi_{ql}(\rho_1) = (\phi_{ql1}, \ldots, \phi_{qlp})^{\mathrm{T}}$ and $\psi_{ql}(r) = (\psi_{ql}^A, \psi_{ql}^D)^{\mathrm{T}}$ and the singular values σ_{ql} are defined by

$$KK^*\phi_{ql} = \sigma_{ql}^2\phi_{ql}, \tag{47}$$

with

$$K^*\phi_{ql} = \sigma_{ql}\psi_{ql}. \tag{48}$$

To obtain the ϕ_{ql}, we rewrite Eq. (47) as

$$\sum_{j=1}^{p} (K_{q_i}^A K_{q_j}^{A*} + K_{q_i}^D K_{q_j}^{D*})\phi_{qlj} = \sigma_{ql}^2\phi_{qli}. \tag{49}$$

Then we use the SVDs (24) and (34) to obtain the identities

$$K_{q_i}^A K_{q_j}^{A*} g_{qq_j} = \chi_{ij}^A(q)\sigma_{qq_i}^A \sigma_{qq_j}^A g_{qq_i}, \tag{50}$$

$$K_{q_i}^D K_{q_j}^{D*} q_{qq_j} = \chi_{ij}^D(q)\sigma_{qq_i}^D \sigma_{qq_j}^D g_{qq_i}. \tag{51}$$

The overlap functions $\chi_{ij}^A(q)$ and $\chi_{ij}^D(q)$ are defined by

$$\langle f_{qq_i}^A, f_{q'q_j}^A \rangle = \chi_{ij}^A(q)\delta(q - q'), \tag{52}$$

$$\langle f_{qq_i}^D, f_{q'q_j}^D \rangle = \chi_{ij}^D(q)\delta(q - q'). \tag{53}$$

Next, we make the ansatz $\phi_{qlj} = c_{lj}(q)g_{qq_j}$ and use Eqs. (49)–(51) to find that the $c_{lj}(q)$ satisfy the equation

$$\sum_j M_{ij}(q)c_{lj}(q) = \sigma_{ql}^2 c_{li}(q), \tag{54}$$

where

$$M_{ij}(q) = \chi_{ij}^A(q)\sigma_{qq_i}^A \sigma_{qq_j}^A + \chi_{ij}^D(q)\sigma_{qq_i}^D \sigma_{qq_j}^d. \tag{55}$$

Note that $c_l(q)$ is an eigenvector of $M_{ij}(q)$ with eigenvalue σ_{ql}^2 and that, since $M_{ij}(q)$ is symmetric, we can choose the $c_l(q)$ to be orthonormal. Finally, we use Eq. (48) to obtain the $\psi_{ql}(r)$, which are given by

$$\psi_{ql}^A(r) = \frac{1}{\sigma_{ql}} \sum_j \sigma_{qq_j}^A c_{lj}(q) f_{qq_j}^A(r), \tag{56}$$

$$\psi^D_{ql}(r) = \frac{1}{\sigma_{ql}} \sum_j \sigma^D_{qq_j} c_{lj}(q) f^D_{qq_j}(r). \tag{57}$$

The solution to Eq. (44) may now be expressed as

$$f(r) = \int \mathrm{d}^2\rho_1 K^+(r, \rho_1)\phi(\rho_1), \tag{58}$$

where

$$K^+(r, \rho_1) = \int \mathrm{d}^2 q \sum_l \frac{1}{\sigma_{ql}} \psi_{ql}(r)\phi^*_{ql}(\rho_1). \tag{59}$$

Using this result, we obtain

$$\delta\alpha(r) = \int \mathrm{d}^2\rho_1 \int \mathrm{d}^2 q \sum_l \frac{1}{\sigma_{ql}} \psi^A_{ql}(r)\phi^*_{ql}(\rho_1)\phi(\rho_1), \tag{60}$$

$$\delta D(r) = \int \mathrm{d}^2\rho_1 \int \mathrm{d}^2 q \sum_l \frac{1}{\sigma_{ql}} \psi^D_{ql}(r)\phi^*_{ql}(\rho_1)\phi(\rho_1), \tag{61}$$

which are the inversion formulas for the inverse scattering problem with diffusing waves.

Several comments on the above results are necessary. First, the solution that we have constructed to the inverse problem is the unique solution of minimum norm given the scattering data. This statement follows from the result that the SVD provides the solution to Eq. (20) that belongs to the orthogonal complement of the null space.[24] It is important to note that the size of the null space is expected to decrease as the number of wave vectors increases, and thus the inversion procedure is systematically improvable. Second, the SVD provides considerable information on the degree of ill-posedness of the inverse problem through the rate of decay of the singular values. It also gives insight into how much information is contained in the data by controlling which features of $\delta\alpha$ and δD can be recovered in a stable way, namely, those that are close to singular functions ψ_{ql} with correspondingly large singular values. Third, as discussed above, although the inverse problem is ill-posed, by introducing an appropriate regularization procedure, we construct a solution that is well behaved. In this context, regularization consists of cutting off the wave-vector integrations in Eqs. (60) and (61) at large $|q|$. Note that regularization here has a natural physical interpretation. It simply sets the transverse spatial resolution of the reconstruction. Fourth, the diffusion imaging experiment is carried out in the near field of the diffusing wave, even though it is the far field of the electromagnetic wave that is measured at the detector. Thus the expectation from geometrical optics that the spatial resolution of the reconstructed image should be controlled by the wavelength of the diffusing wave does not hold.

C. Iterative Multiple-Wave-Vector Solutions

We now consider an alternative approach to the multiple-wave-vector inverse problem. Rather than solving the integral equations (43) by SVD, we obtain the solution by an iterative method. It is useful to rewrite Eq. (43) as

$$K_{q_i} f = \phi_{q_i}, \tag{62}$$

where the vector operator $K_{q_i} = (K^A_{q_i}, K^D_{q_i})$. To solve Eq. (62), we introduce the orthogonal projection operators P_i onto the affine subspace $\mathcal{F}_i = \{f : K_{q_i} f = \phi_{q_i}\}$. Then the solution to Eq. (62) can be obtained by successive projections onto the $\mathcal{F}_i$, thereby defining a sequence of functions f_n that converges to the solution to Eq. (62). Thus the solution to Eq. (62) is given by

$$f_{n+1} = \prod_i P_i f_n, \tag{63}$$

with $n = 1, 2, \ldots$ and f_1 arbitrary. To make further progress, we require an explicit form for the projection operator P_i. This is given by

$$P_i f = f + K^*_{q_i}(K_{q_i} K^*_{q_i})^{-1}(\phi_{q_i} - K_{q_i} f). \tag{64}$$

Using this result and Eq. (63), we obtain the recursion relation

$$f^{i+1}_n = f^i_n + K^*_{q_i}(K_{q_i} K^*_{q_i})^{-1}(\phi_{q_i} - K_{q_i} f^i_n), \tag{65}$$

where $f^1_n \equiv f_n$ and $f^{p+1}_n \equiv f_{n+1}$. We now rewrite Eq. (65) as

$$\delta\alpha^{i+1}_n = \delta\alpha^i_n + K^{A*}_{q_i}(K^A_{q_i} K^{A*}_{q_i} + K^D_{q_i} K^{D*}_{q_i})^{-1} \times (\phi_{q_i} - K^A_{q_i}\delta\alpha^i_n - K^D_{q_i}\delta D^i_n), \tag{66}$$

$$\delta D^{i+1}_n = \delta D^i_n + K^{D*}_{q_i}(K^A_{q_i} K^{A*}_{q_i} + K^D_{q_i} K^{D*}_{q_i})^{-1} \times (\phi_{q_i} - K^A_{q_i}\delta\alpha^i_n - K^D_{q_i}\delta D^i_n). \tag{67}$$

Finally, we use the SVDs of $K^A_{q_i}$ and $K^D_{q_i}$ to obtain

$$\delta\alpha^{i+1}_n(r) = \delta\alpha^i_n(r) + \int \mathrm{d}^2\rho_1 \int \mathrm{d}^2 q\, \sigma^A_{qq_i}[(\sigma^A_{qq_i})^2 + (\sigma^D_{qq_i})^2]^{-1} g^*_{qq_i}(\rho_1) f^A_{qq_i}(r)[\phi_{q_i}(\rho_1) - K^A_{q_i}\delta\alpha^i_n(\rho_1) - K^D_{q_i}\delta D^i_n(\rho_1)], \tag{68}$$

$$\delta D^{i+1}_n(r) = \delta D^i_n(r) + \int \mathrm{d}^2\rho_1 \int \mathrm{d}^2 q\, \sigma^D_{qq_i}[(\sigma^A_{qq_i})^2 + (\sigma^D_{qq_i})^2]^{-1} g^*_{qq_i}(\rho_1) f^D_{qq_i}(r)[\phi_{q_i}(\rho_1) - K^A_{q_i}\delta\alpha^i_n(\rho_1) - K^D_{q_i}\delta D^i_n(\rho_1)], \tag{69}$$

which provides an iterative solution to the inverse scattering problem with diffusing waves. Observe that each iteration of the inversion procedure is computed analytically and is similar in form to that of the single-wave-vector case considered above. Note that the computational complexity per iteration is $O(N \log N)$, where N is the number of source–detector pairs. This should be compared with the $O(N^2)$ complexity of numerical iterative algorithms such as the algebraic reconstruction technique.[24] Implementation of this algorithm will be presented elsewhere.

4. NUMERICAL RESULTS AND DISCUSSION

A. General Comments on the Reconstruction Algorithm

To illustrate the inversion formulas derived in this paper, we consider a few numerical examples. Namely, we will apply the multiple-wave-vector solutions obtained in Subsection 4.B. As follows from Eqs. (60) and (61), after substitution of the explicit expressions for the singular functions, the inversion formulas for $\delta\alpha$ and δD can be rewritten as

$$\delta\alpha(r) = \left(\frac{D_0}{\pi}\right)^2 \int \mathrm{d}^2 q \, \exp(iq \cdot \rho) \times \sum_{k,l} \eta^A(z;q,q_k) A_{kl}^{-1}(q) \zeta(q,q_l), \quad (70)$$

$$\delta D(r) = \left(\frac{D_0}{\pi}\right)^2 \int \mathrm{d}^2 q \, \exp(iq \cdot \rho) \times \sum_{k,l} \eta^D(z;q,q_k) A_{kl}^{-1}(q) \zeta(q,q_l), \quad (71)$$

where we have used the following notation:

$$\eta^A(z;q,q_k) = \exp\{-[Q^*(q_k) + Q^*(q+q_k)]z\}, \quad (72)$$

$$\eta^D(z;q,q_k) = t^*(q_k,q)\exp\{-[Q^*(q_k) + Q^*(q+q_k)]z\}, \quad (73)$$

$$\zeta(q,q_k) = Q(q_k)Q(q_k+q)\hat{\phi}(-(q_k+q),q_k), \quad (74)$$

$$A_{kl}(q) = \frac{1 - \exp\{[Q(q_k) + Q(q_k+q) + Q^*(q_l) + Q^*(q_l+q)]L\}}{Q(q_k) + Q(q_k+q) + Q^*(q_l) + Q^*(q_l+q)}[1 + t(q_k,q)t^*(q_l,q)], \quad (75)$$

$$t(q_k,q) = q_k \cdot (q_k+q) + Q(q_k)Q(q_k+q), \quad (76)$$

and $\hat{\phi}(q_1,q_2)$ is the Fourier transform of the scattering data $\phi(\rho_1,\rho_2)$.

Several comments on the above equations are necessary. First, they were obtained under the assumption that $\delta\alpha$ and δD are nonzero only for $0 \leq z \leq L$. This corresponds to the experimental situation in which the object to be imaged is spatially confined. It also improves the numerical stability of the reconstruction. Mathematically, the consequence of this assumption is that the spatial integrals in the inner products defining the $\chi_{ij}(q)$'s must be evaluated in the region $0 \leq z \leq L$. Note that the limit $L \to \infty$ is well defined, since the real part of the exponential factor in Eq. (75) is positive. Second, the expression $A_{ij}^{-1}(q) = \Sigma_l c_{li}^*(q) c_{lj}(q)/\sigma_{ql}^2$. In fact, although the matrix A is nonnegative definite, many of its eigenvalues are extremely small. As a result, inversion of A is not well defined numerically. However, diagonalization of A is numerically stable. Therefore we use the above expansion of A^{-1}, where the terms with singular values σ_{ql} smaller than a certain threshold ϵ are not included. This procedure is mathematically analogous to regularization of the SVD and is crucial for the calculations reported here. Finally, it is important to appreciate that an image reconstruction algorithm based on Eqs. (70) and (71) has, with the use of the fast Fourier transform, computational complexity $O(N \log N)$, where N is the number of source–detector paris. This should be compared with the $O(N^3)$ complexity of a direct numerical inversion of the integral equation (15).

The set of two-dimensional vectors q_k is, in principle, arbitrary. Theoretically, by using a larger number of q_k's, the inverse problem should become better conditioned. In practice, however, when the dimension of A increases, the number of singular values that are above the threshold ϵ tends to remain constant. Therefore the number of useful q_k's is limited. In our numerical examples, we used a set of approximately 40 q_k's, all of which were collinear. This choice avoids some additional degeneracies of A, which originate from the invariance of A with respect to the transformation $q_k \to -q_k + 2(q_k q)/q/q^2$.

The inversion formulas (70) and (71) use the Fourier-transformed rather than the real-space scattering data. Theoretically, both descriptions are equivalent. However, in practice, the calculation of the Fourier-transformed scattering data is limited by the number of source–detector pairs. In the examples reported here, we demonstrate the feasibility of the SVD reconstruction algorithms and avoid the numerical errors associated with a finite number of source–detector pairs. This is achieved by solving the forward problem and obtaining $\phi(q_1,q_2)$ analytically. For this purpose we employed the solution to the forward-scattering problem produced by a finite number of pointlike absorbers and scatterers:

$$\delta\alpha(r) = \sum_{k=1}^{N_A} \alpha_k \delta(r - r_k^A), \quad (77)$$

$$\delta D(r) = \sum_{k=1}^{N_D} D_k \delta(r - r_k^D). \quad (78)$$

Here N_A and N_D are the numbers of absorbers and scatterers, respectively, and $r_k^{A(D)}$ are the coordinates of absorbers (scatterers). We stress that the coordinates of the absorbers and scatterers are used only for the forward problem calculation and that no *a priori* information about $\delta\alpha$ or δD is used in the inversion procedure. Note also that the images obtained from the forward data calculated in this way demonstrate the resolution of point objects.

The Fourier-transformed forward data for $\delta\alpha$ and δD given by Eqs. (77) and (78) can be easily obtained from Eq. (18):

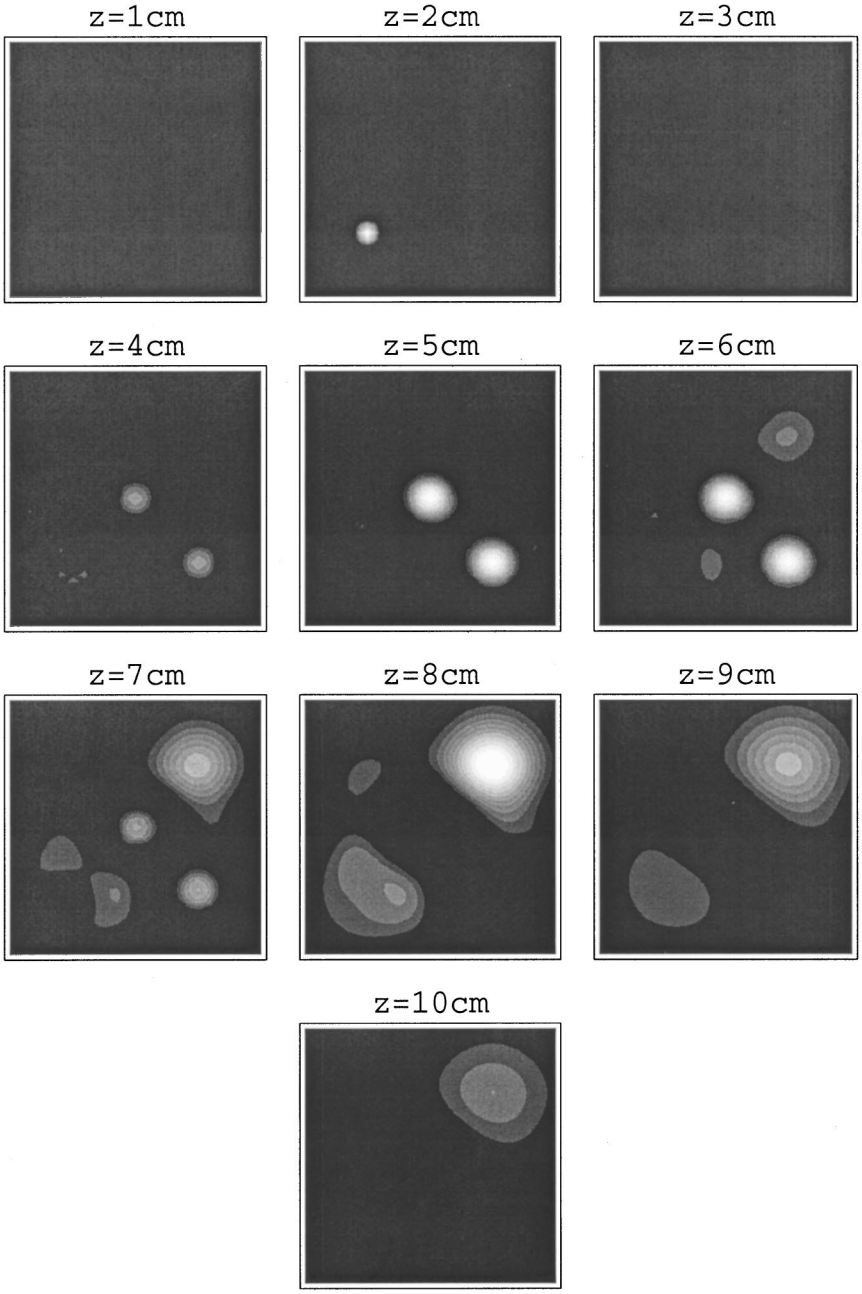

Fig. 4. Tomographic images of four pointlike absorbers. The longitudinal ranges of the tomographic slices (all lengths are in centimeters) are $-10 \leqslant x, y \leqslant 10$. The coordinates of absorbers are $x = -5$, $y = -5$,$z = 2$ (lower left corner); $x = 0$, $y = 0$, $z = 5$ (center); $x = 5, y = -5, z = 5$ (lower right corner); and $x = 5, y = 5, z = 8$ (upper right corner). The reconstruction is done for zero modulation frequency ($\omega = 0$) with wavelength $\lambda = 2\pi/k_0 = 10$. The images are calibrated from 0 (black) to 1 (white) in absolute scale. Here black corresponds to $\delta\alpha = 0$ and white to the maximum absolute value of $\delta\alpha$ obtained for a pointlike absorber located at a particular depth.

$$\hat{\phi}(-(q_k + q), q_k) = \frac{1}{(2D_0)^2 Q(q_k) Q(q_k + q)} \Bigg(\sum_{l=1}^{N_A} \alpha_l \exp\{-iq \cdot \rho_l^A - [Q(q_k) + Q(q_k + q)] z_l^A\} + t(q_k, q) \sum_{l=1}^{N_D} D_l \times \exp\{-iq \cdot \rho_l^D - [Q(q_k) + Q(q_k + q)] z_l^D\} \Bigg). \tag{79}$$

Our numerical procedure consists of the following steps:

- Generate the forward solution for a fixed number of pointlike absorbers and scatterers.
- Define a set of two-dimensional vectors q_k and q [the latter are used in numerical integration over d^2q according to Eqs. (70) and (71)].
- Generate the fields $\eta(z; q, q_k)$ and $\zeta(q, q_k)$ for the values of q_k and q determined previously.
- Integrate over d^2q. For each value of q, the matrix

$A(q)$ is diagonalized, and the inner product $\langle \eta, A^{-1}\zeta \rangle$ is calculated by using the regularization procedure (only singular values with $\sigma_{ql} > \epsilon$ are included in the summation).

Note that $A(q)$ does not depend on the scattering data. Therefore, for given discrete values of q and q_k, diagonalization of A is performed only once, even for multiple reconstructions.

B. Reconstruction of $\delta\alpha$

We start with the reconstruction of $\delta\alpha$ when δD is assumed to be zero. We considered the simplest case of a cw experiment with the "wavelength" of the diffusing wave as $\lambda = 2\pi/k_0 = 10$ cm. This value of k_0 is typical for human tissue with near-infrared light.

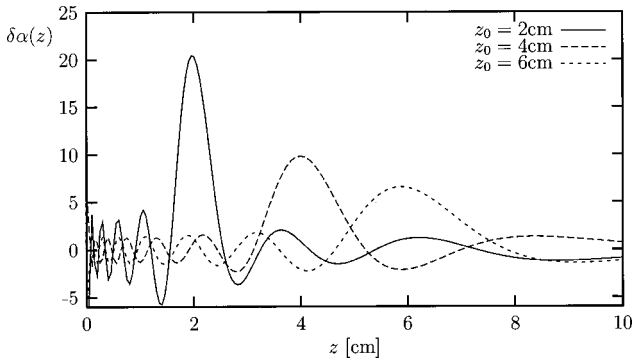

Fig. 5. Reconstruction in a one-dimensional geometry with infinitely thin plane absorbers located at different depths z_0.

Since k_0 is real in a cw experiment, the matrix A is real and symmetric. Therefore we used Jacobi diagonalization, which is fast and robust numerically, to calculate its eigenvalues (σ_{ql}^2) and eigenvectors $[c_{ln}(q)]$. The regularization constant ϵ was chosen to be 10^{-18}. The optimum value of ϵ depends on the numerical precision of the code and other computational details, such as the off-diagonal norm tolerance in the Jacobi diagonalization process. We have used 40 collinear wave vectors q_k ranging in absolute length from 0 to 40 cm^{-1}, all in the $\hat{x}$ direction. It may be shown, however, that the reconstructed images are essentially independent of the direction of this line. The same results may also obtained when the q_k are not collinear but fill a square. Integration over d^2q was carried out numerically by using the simple trapezoidal rule for $q_{x,y}$ ranging from -40 to 40 cm^{-1} with a step of 1 cm^{-1}. The transverse dimensions of the sample were taken to be 20 cm $\times$ 20 cm, and the depth $L = 10$ cm.

The reconstructed images are shown in Fig. 4. Four pointlike absorbers were used to generate the forward data: one in the $z = 2$ cm plane, two in the $z = 5$ cm plane, and one in the $z = 8$ cm plane. The tomographic slices clearly illustrate the depth dependence of the resolution. The first absorber, at $z = 2$ cm, is clearly re-

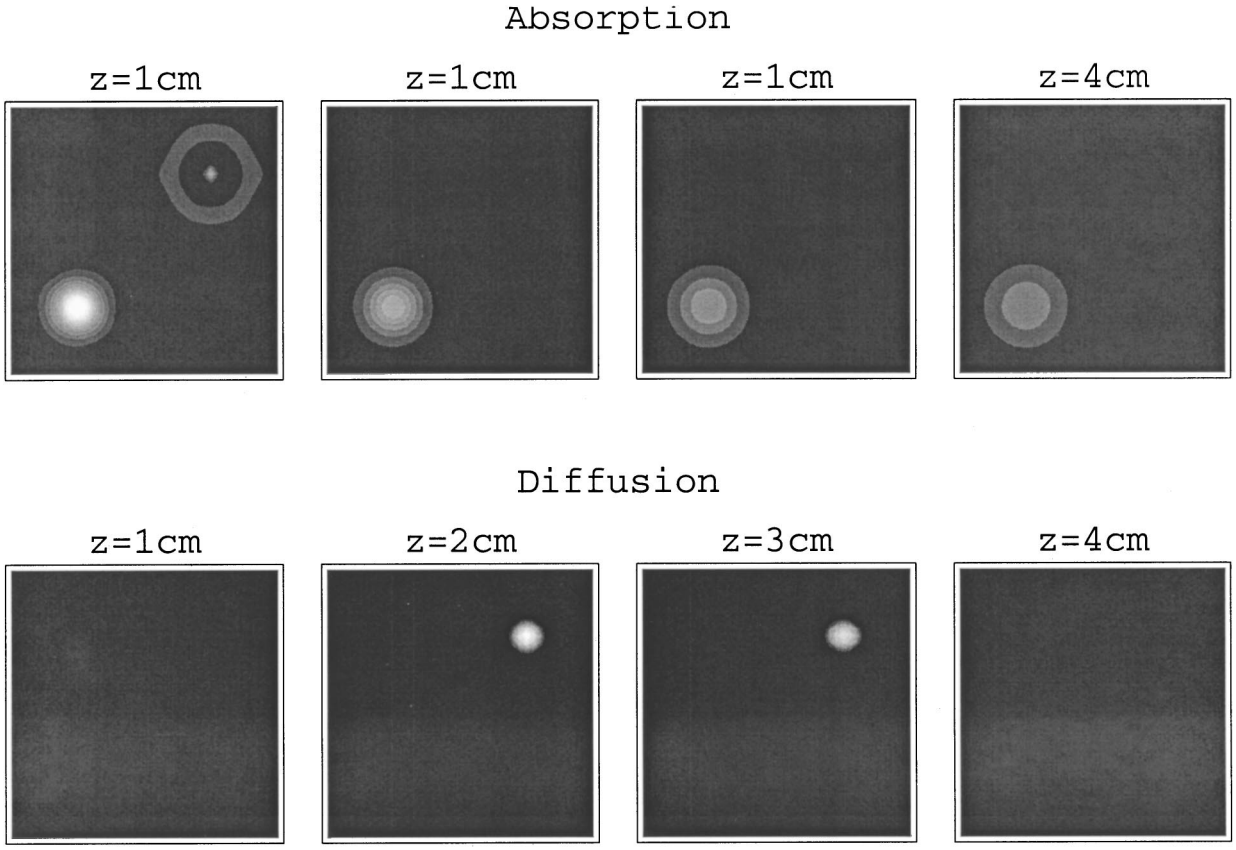

Fig. 6. Simultaneous reconstruction of $\delta\alpha$ and δD for one point absorber and one point scatterer, both located at the depth $z = 2$ (all lengths are in centimeters). The absorber is located in the lower left corner ($x = -5, y = -5, z = 2$); the scatterer is located in the upper right corner ($x = 5, y = 5, z = 2$). Other parameters are the same as those in Fig. 4. The images for $\delta\alpha$ are not calibrated, since reconstructed $\delta\alpha$ has no maxima in the z direction; calibration of δD images is done as in Fig. 4.

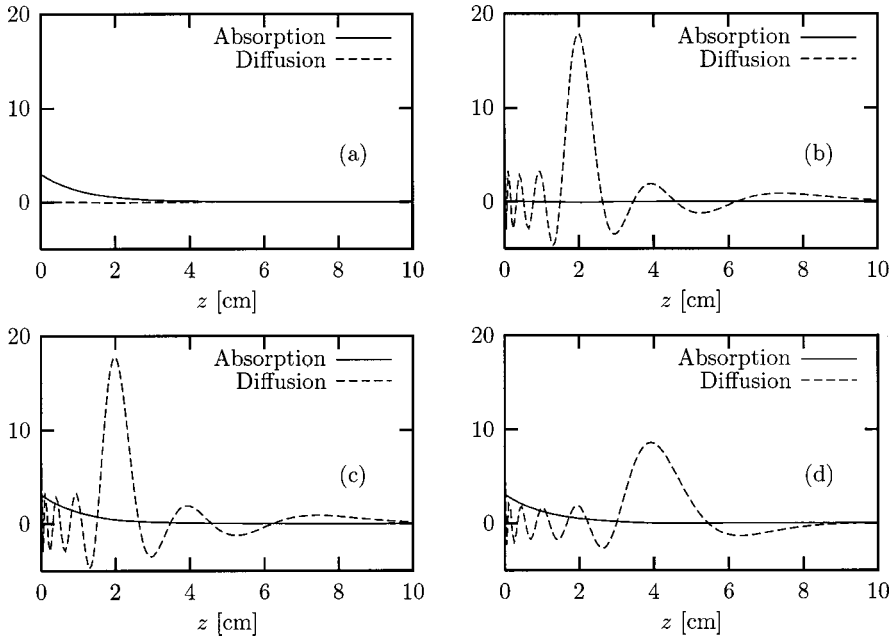

Fig. 7. Reconstruction in a one-dimensional geometry for different infinitely thin absorbers and scatterers: (a) one absorber at $z = 2$ cm; (b) one scatterer at $z = 2$ cm; (c) one absorber and one scatterer, both at $z = 2$ cm; (d) one absorber at $z = 2$ cm and one scatterer at $z = 4$ cm.

solved, both in the xy plane and in the z direction. Note that the tomographic slices at $z = 7$, 8, and 9 cm show traces of the three absorbers that are located at $z = 2$ and 5 cm. Generally, for depths $z > \lambda$ the resolution is very poor (data not shown).

To illustrate the nature of the depth resolution, we have performed reconstructions in the one-dimensional geometry where $\delta\alpha$ depends only on z. The analog of a point in this case is an infinitely thin plane absorber located at a depth z_0 with $\delta\alpha(z) = \alpha_0\delta(z - z_0)$. The forward-scattering data in this case are given by

$$\hat{\phi}(-(q_k + q), q_k) = \alpha_0\left(\frac{\pi}{D_0}\right)^2 \frac{\delta(q)\exp[-2Q(q_k)]}{Q^2(q_k)}. \tag{80}$$

The reconstructed profile of $\delta\alpha(z)$ is shown in Fig. 5 for different values of z_0.

The reconstruction of δD with $\delta\alpha$ assumed to be zero results in images that are very similar to those shown in this section. Note that when the Fourier-transformed scattering data are known analytically, the inversion formulas in both cases can be shown to be mathematically equivalent.

To summarize, both the lateral and depth resolutions decrease with depth. This result is expected, since diffusing waves decay exponentially with depth, limiting the range of accessible transverse wave vectors in the inversion formulas (70) and (71). However, reasonable resolution can be obtained for $z < \lambda$, with λ as the diffuse wavelength.

C. Simultaneous Reconstruction of $\delta\alpha$ and δD

Now we turn to the simultaneous reconstruction of $\delta\alpha$ and δD. Reconstructed images of one pointlike absorber and one pointlike scatterer located in the $z = 2$ cm plane are shown in Fig. 6. In this case both the lateral and depth resolutions for δD are approximately the same as those in Fig. 4. However, the resolution in the $\delta\alpha$ images is substantially worse. As can be seen from the figure, the slice where $\delta\alpha$ has maximum intensity does not coincide with the location of the absorber. Nevertheless, some transverse resolution is retained, and an absorbing inhomogeneity can be, in principle, detected in this setting.

The difference in the resolution for $\delta\alpha$ and δD can be understood as follows. The problem of reconstructing two functions from one integral equation is essentially underdetermined. In the integral equation that couples $\delta\alpha$ and δD, the part proportional to δD is multiplied by a factor $t(q_k, q)t^*(q_l, q)/k^2$. This term is almost always much larger than unity. As a result, precision is retained in the reconstruction of δD but lost for $\delta\alpha$.

The above feature of simultaneous reconstruction of $\delta\alpha$ and δD can be easily seen in the one-dimensional geometry described at the end of Subsection 4.B. In Fig. 7 we show reconstructed images of $\delta\alpha$ and δD for infinitely thin absorbing and scattering planes that are parallel to the $z = 0$ plane. In Fig. 7(a) the forward data are generated by only one absorbing plane at $z = 2$ cm. Evidently, the image indicates the presence of an absorbing inhomogeneity and the absence of a diffusing inhomogeneity; however, the exact location of the absorbing plane cannot be determined from this image. In Fig. 7(b) the forward data are generated by only one scattering plane at the same depth, $z = 2$ cm. In this case the location of the scattering plane can be determined with high resolution. Finally, Fig. 7(c) shows images of one absorbing and one scattering plane located at the same depth, and Fig. 7(d) does so at different depths.

We note that the resolution for simultaneous recon-

struction of $\delta\alpha$ and δD can be improved in experiments involving two different modulation frequencies. The SVD can be easily generalized to the case of two-frequency measurements. Indeed, the inversion formulas (70) and (71) can be written in terms of the variables $p_k(q, k_0) = Q(q_k) + Q(q_k + q)$. In a one-frequency experiment, the number of different p_k's is the same as the number of vectors q_k. Using an additional modulation frequency is equivalent to doubling the number of mathematically independent variables p_k while keeping the number of vectors q_k constant. Thus the rank of the matrix A is effectively doubled, which makes the inverse problem better conditioned.

In conclusion, we have described an inverse scattering method for reconstructing the optical absorption and diffusion coefficients of a highly scattering medium probed by diffusing waves. We emphasize that our approach represents an analytic rather than a numerical solution to the image reconstruction problem. The results of this investigation are of general physical interest, since they are applicable to imaging with any multiply scattered scalar wave in the diffusion regime.

ACKNOWLEDGMENTS

The authors are grateful to P. Scott Carney for valuable discussions. This work was supported in part by the National Institutes of Health.

Address correspondence to John Schotland, Department of Electrical Engineering, Campus Box 1127, Washington University, One Brookings Drive, St. Louis, Missouri 63130-4899, or by e-mail: jcs@ee.wustl.edu.

REFERENCES

1. G. J. Mueller, B. Chance, R. R. Alfano, S. R. Arridge, J. Beuthan, E. Gratton, M. Kaschke, B. R. Masters, S. Svanberg, and P. van der Zee, eds., *Medical Optical Tomography: Functional Imaging and Monitoring* (SPIE Press, Bellingham, Wash., 1993).
2. R. R. Alfano and J. G. Fujimoto, eds., *Advances in Optical Imaging and Photon Migration*, Vol. 2 of OSA Trends in Optics and Photonics Series (Optical Society of America, Washington, D.C., 1996).
3. B. Chance and R. R. Alfano, eds., *Optical Tomography and Spectroscopy of Tissue and Model Media: Theory, Human Studies, and Instrumentation*, Proc. SPIE **2389** (1995).
4. B. Chance and R. R. Alfano, eds., *Optical Tomography and Spectroscopy of Tissue and Model Media: Theory, Instrumentation, and Human Studies II*, Proc. SPIE **2949** (1997).
5. B. Chance, R. R. Alfano, and B. Tromberg, eds, *Optical Tomography and Spectroscopy of Tissue III*, Proc. SPIE **3597**, (1999).
6. M. C. W. van Rossum and T. M. Nieuwenhuizen, "Multiple scattering of classical waves: microscopy, mesoscopy and diffusion," Rev. Mod. Phys. **71**, 313–371 (1999).
7. S. R. Arridge, "Optical tomography in medical imaging," Inverse Probl. **15**, R41–R93 (1999).
8. L. Wang, P. P. Ho, C. Liu, G. Zhang, and R. R. Alfano, "Ballistic 2-D imaging through scattering walls using an ultrafast optical Kerr gate," Science **253**, 769–771 (1991).
9. D. A. Benaron and D. K. Stevenson, "Optical time-of-flight and absorbance imaging of biologic media," Science **259**, 1463–1466 (1993).
10. A. Rebane and J. Feinberg, "Time-resolved holography," Nature (London) **351**, 378–380 (1991).
11. K. M. Yoo, F. Liu, and R. R. Alfano, "Imaging objects hidden in scattering media using an absorption technique," Opt. Lett. **16**, 1068–1070 (1991).
12. E. Leith, H. Chen, Y. Chen, D. Dilworth, J. Lopez, R. Masri, J. Rudd, and J. Valdmanis, "Electronic holography and speckle methods for imaging through tissue using femtosecond gated pulses," Appl. Opt. **30**, 4204–4210 (1991).
13. E. N. Leith, B. G. Hoover, D. S. Dilworth, and P. P. Naulleau, "Ensemble-averaged Shack–Hartmann wavefront sensing for imaging through turbid media," Appl. Opt. **37**, 3643–3650 (1998).
14. J. R. Singer, F. A. Grunbaum, P. Kohn, and J. P. Zubelli, "Image reconstruction of the interior of bodies that diffuse radiation," Science **248**, 990–993 (1990).
15. S. R. Arridge, P. van der Zee, M. Cope, and D. T. Delpy, "New results for the development of infrared absorption imaging," in *Biomedical Image Processing*, A. C. Bovik and W. E. Higgins, eds., Proc. SPIE **1245**, 92–103 (1991).
16. R. L. Barbour, H. L. Graber, R. Aronson, and J. Lubowsky, "Imaging of subsurface regions of random media by remote sensing," in *Time-Resolved Spectroscopy and Imaging of Tissues*, B. Chance and A. Katzin, eds., Proc. SPIE **1431**, 192–203 (1991).
17. J. Schotland and J. Leigh, "Photon diffusion imaging," Biophys. J. **61**, 446 (1992).
18. C. P. Gonatas, M. Ishii, J. S. Leigh, and J. C. Schotland, "Optical diffusion imaging using a direct inversion method," Phys. Rev. E **52**, 4361–4365 (1995).
19. M. Ishii, J. Leigh, and J. Schotland, "Photon diffusion imaging of model and biological systems," in *Optical Tomography, Photon Migration, and Spectroscopy of Tissue and Model Media: Theory, Human, Studies, and Instrumentation*, B. Chance and R. R. Alfano, eds., Proc. SPIE **2389**, 312–317 (1995).
20. M. O'Leary, D. Boas, B. Chance, and A. Yodh, "Experimental images of heterogeneous turbid media by frequency-domain diffusing photon tomography," Opt. Lett. **20**, 426–429 (1995).
21. J. C. Schotland, "Continuous wave diffusion imaging," J. Opt. Soc. Am. A **14**, 275–279 (1997).
22. X. D. Li, T. Durduran, A. Yodh, B. Chance, and D. Pattanayak, "Diffraction tomography for biochemical imaging with diffuse photon density waves," Opt. Lett. **22**, 573 (1997).
23. C. Matson, "A diffraction tomographic model of the forward problem using photon density waves," Opt. Express **1**, 6–11 (1997).
24. F. Natterer, *The Mathematics of Computerized Tomography* (Wiley, New York, 1986).